

# Driven-Dissipative Interpretation of Measurement-Induced State Transitions Beyond Semiclassical Predictions

Bo-Syun Pan,<sup>1</sup> Yen-Hsiang Lin,<sup>2</sup> and Chiao-Hsuan Wang<sup>1,3,4,\*</sup>

<sup>1</sup>*Department of Physics and Center for Theoretical Physics,  
National Taiwan University, Taipei 106319, Taiwan*

<sup>2</sup>*Department of Physics, National Tsing Hua University, Hsinchu 300013, Taiwan*

<sup>3</sup>*Center for Quantum Science and Engineering, National Taiwan University, Taipei 106319, Taiwan*

<sup>4</sup>*Physics Division, National Center for Theoretical Sciences, Taipei 106319, Taiwan*

Dispersive readout plays a central role in superconducting quantum computing, enabling quantum nondemolition (QND) measurements of qubits through a coupled microwave resonator. However, under strong readout drives, multi-photon resonances can cause measurement-induced state transition (MIST), resulting in qubit leakage out of the computational subspace and compromising the QND character. We present a driven-dissipative interpretation of MIST using a reduced quantum model that captures the dynamics and entanglement structure underlying the breakdown of QND measurement, a feature inaccessible to previous semiclassical treatments. A super-MIST regime under strong drive is uncovered, characterized by steady-state qubit inversion and slow relaxation beyond the semiclassical Landau-Zener predictions. We further identify a transient readout condition in which the resonator becomes highly populated while the qubit remains near its original state. These results are broadly applicable to superconducting qubits such as fluxonium and transmon, unveil the nonequilibrium dynamics of MIST, and highlight strongly driven regimes that can be leveraged for measurement optimization.

## INTRODUCTION

Superconducting circuits have been established as one of the leading platforms for quantum computing hardware [1, 2], where microwave resonators enable high-fidelity control and readout of artificial atoms in the circuit quantum electrodynamics architecture [3]. In particular, quantum nondemolition (QND) measurement of superconducting qubits can be implemented via dispersive readout, where the qubit induces a state-dependent frequency shift on a coupled microwave resonator, enabling high-fidelity state inference without directly perturbing the qubit [4, 5]. While increasing the drive strength generally improves readout contrast through increased resonator photon number, various experiments have observed leakage into noncomputational qubit states under strong driving [6–10], indicating a breakdown of the dispersive regime and the associated QND behavior. This phenomenon is commonly termed measurement-induced state transition (MIST) [6, 11–13], or qubit ionization [9, 14–16].

Multi-photon resonances between computational and higher excited qubit states have been identified as the primary mechanism behind such transitions [6]. These processes were recently captured by full quantum models that treat the exact qubit spectrum and the driven bosonic resonator beyond the dispersive approximation [15]. However, simulating such models remains computationally demanding due to the large Hilbert space of the coupled nonlinear multilevel qubit-resonator system and the explicit time dependence of the drive. Moreover, numerical simulations alone offer limited physical insight into the mechanisms underlying these transitions.

To explore MIST behavior using tractable approximations, simplified quantum metrics such as qubit purity or dressed matrix elements have been proposed to qualitatively predict its onset [12, 16]. For quantitative predictions, most studies adopt semiclassical approaches that replace the resonator field with a coherent amplitude [9, 11, 14, 15]. Despite offering computational efficiency, semiclassical models neglect the quantum nature of the resonator and consequently omit the qubit-resonator entanglement responsible for the breakdown of QND behavior, leading to discrepancies in the predicted MIST dynamics. These limitations warrant an efficient quantum model that can capture both the quantitative behavior and the underlying physics of MIST beyond semiclassical approximations.

Here we present a reduced quantum model that captures measurement-induced state transitions through driven-dissipative nonequilibrium dynamics, offering analytical access to both transient and steady-state behavior. In particular, we identify the emergence of a super-MIST regime, defined by steady-state qubit inversion above a strong-drive threshold, where semiclassical approaches deviate significantly from quantum predictions due to their neglect of qubit-resonator entanglement. Within this regime, we further reveal a finite-time operating condition where the qubit remains near its original state while the resonator becomes highly populated, enabling fast, high-fidelity dispersive readout beyond semiclassical reach. These results elucidate the nonequilibrium dynamics underlying the breakdown of QND behavior and establish an efficient framework for optimizing qubit readout protocols.

## QUANTUM MODEL

We begin with the full quantum model of a nonlinear superconducting qubit capacitively coupled to a driven microwave resonator [15], schematized in Fig. 1(a). While applicable to generic superconducting qubits, we focus on fluxonium for concrete modeling with realistic experimental parameters[17, 18]. The qubit Hamiltonian is given by (taking  $\hbar = 1$ )

$$\hat{H}_q = 4E_C\hat{n}^2 + \frac{1}{2}E_L\hat{\varphi}^2 - E_J \cos(\hat{\varphi} - \varphi_{\text{ext}}), \quad (1)$$

where  $\hat{\varphi}, \hat{n}$  are the normalized flux and charge operators of the fluxonium qubit, satisfying  $[\hat{\varphi}, \hat{n}] = i$ . The parameters  $E_C$ ,  $E_L$ , and  $E_J$  denote the charging, inductive, and Josephson energies, respectively. The external flux is given by  $\varphi_{\text{ext}} = 2\pi\Phi_{\text{ext}}/\Phi_0$ , where  $\Phi_0$  is the magnetic flux quantum. Numerical values of physical parameters used in this work are listed in Table I. The qubit Hamiltonian can be diagonalized as  $\hat{H}_q = \sum_{j=0} \omega_j |j\rangle\langle j|$ , where  $|j\rangle$  denotes the  $j$ -th qubit eigenstate, yielding a nonlinear energy spectrum as shown in Fig. 1(b).

$E_C/h$	4.43 GHz	$\omega_r/2\pi$	5.9436 GHz
$E_J/h$	0.795 GHz	$\omega_d/2\pi$	5.9436 GHz
$E_L/h$	0.89 GHz	$\kappa/2\pi$	4.086 MHz
$g/2\pi$	0.098 GHz	$\varphi_{\text{ext}}$	0.010

TABLE I. Physical parameters based on experimentally realistic values for fluxonium readout devices.

The full system Hamiltonian is  $\hat{H}_{\text{full}}(t) = \hat{H}_{qr} + \hat{H}_d(t)$ , where the static qubit–resonator Hamiltonian reads

$$\hat{H}_{qr} = \omega_r \hat{a}^\dagger \hat{a} + \hat{H}_q + ig\hat{n}(\hat{a}^\dagger - \hat{a}). \quad (2)$$

Here,  $\omega_r$  is the bare frequency of the resonator, and  $ig\hat{n}(\hat{a}^\dagger - \hat{a})$  represents the capacitive coupling between the qubit and the resonator with strength  $g$ . The resonator is driven by a classical measurement field, modeled as a time-dependent drive Hamiltonian

$$\hat{H}_d(t) = -2i\varepsilon_d(t) \sin(\omega_d t)(\hat{a}^\dagger - \hat{a}), \quad (3)$$

where  $\omega_d$  and  $\varepsilon_d$  are the drive frequency and the drive amplitude, respectively.

In the limit  $|g| \ll |\Delta|$ ,  $\Delta \equiv \omega_q - \omega_r$ ,  $\omega_q \equiv \omega_1 - \omega_0$ , and assuming low photon occupation in the resonator, the system reduces to the standard dispersive coupling form when restricted to the dressed computational qubit subspace  $|0\rangle = |g\rangle$  and  $|1\rangle = |e\rangle$  [4],

$$\hat{H}_{qr} \approx \omega'_r \hat{a}^\dagger \hat{a} + \omega'_q |e\rangle\langle e| + \chi \hat{a}^\dagger \hat{a} |e\rangle\langle e|, \quad (4)$$

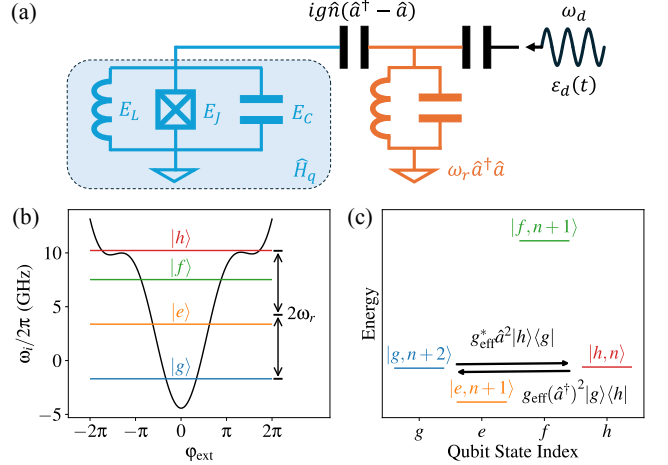


FIG. 1. (a) Schematic of dispersive qubit readout setup, where a fluxonium qubit is capacitively coupled to a microwave resonator driven by a classical field. (b) Nonlinear energy spectrum of the fluxonium qubit. The transition between the ground and third excited states is near two-photon resonance with the readout resonator. (c) Effective two-photon transition between  $|g, n+2\rangle$  and  $|h, n\rangle$  in the reduced model, where  $n$  is the resonator photon number. Other off-resonant states are neglected under the rotating wave approximation.

where  $\omega'_r$  and  $\omega'_q$  are the shifted frequencies and  $\chi = g^2/\Delta$  is the dispersive coupling strength. In this regime, the resonator acquires a qubit-state-dependent frequency shift, enabling quantum nondemolition (QND) measurement of the qubit state through the readout drive [5].

At higher photon numbers, multi-photon processes can drive the qubit out of the computational subspace into higher excited states. For the parameters considered here, the dominant channel is a two-photon resonance between  $|g\rangle = |0\rangle$  and  $|h\rangle = |3\rangle$  at  $2\omega_r \approx \omega_h - \omega_g$  [Fig. 1(b)], which induces qubit–resonator entanglement and thereby breaks the QND readout character. However, the full quantum model is analytically intractable and numerically costly due to the large Hilbert space and time-dependent drive, posing challenges for understanding MIST dynamics. We therefore develop a reduced framework that captures the dynamics and entanglement structure underlying MIST.

Under the generalized dispersive condition that all qubit transitions remain far detuned from the resonator frequency,  $|g\langle i|\hat{n}|j\rangle| \ll |\omega_j - \omega_i - \omega_r|$  for all  $|i\rangle, |j\rangle$ , we perform a Schrieffer–Wolff (SW) transformation together with the rotating-wave approximation to obtain an effective description restricted to the near-resonant subspace [Fig. 1(c)]. The resulting Hamiltonian of the reduced quantum model reads [19]

$$\begin{aligned} \hat{H}_{\text{eff}} = & \delta_a \hat{a}^\dagger \hat{a} + (\delta_g + \chi_g \hat{a}^\dagger \hat{a}) |g\rangle\langle g| + (\delta_h + \chi_h \hat{a}^\dagger \hat{a}) |h\rangle\langle h| \\ & + g_{\text{eff}}(\hat{a}^\dagger)^2 |g\rangle\langle h| + g_{\text{eff}}^*(\hat{a}^\dagger)^2 |h\rangle\langle g| + \varepsilon_d(\hat{a} + \hat{a}^\dagger), \end{aligned} \quad (5)$$

where  $\delta_{a,g,h}$  denote the shifted level energies,  $\chi_{g/h}$  are dispersive couplings, and  $g_{\text{eff}}$  is the effective two-photon coupling strength. This effective Hamiltonian  $\hat{H}_{\text{eff}}$  is expressed in the dressed-state basis defined by the SW transformation and under the rotating frame.

The effective Hamiltonian resembles a two-photon Jaynes–Cummings interaction [20], augmented by dispersive coupling terms and effective level shifts induced by the full qubit spectrum, faithfully captures the full system dynamics. The open-system dynamics within this reduced subspace, including resonator photon loss at rate  $\kappa$ , is governed by the Lindblad master equation

$$\partial_t \hat{\rho} = -i[\hat{H}_{\text{eff}}, \hat{\rho}] + \kappa \mathcal{D}[\hat{a}](\hat{\rho}), \quad (6)$$

where  $\hat{\rho}$  is the density matrix and  $\mathcal{D}[\hat{a}](\hat{\rho}) \equiv \hat{a}\hat{\rho}\hat{a}^\dagger - \frac{1}{2}(\hat{a}^\dagger\hat{a}, \hat{\rho})$  is the Lindblad dissipator.

This reduced description highlights the two-photon qubit–resonator coupling responsible for measurement-induced transitions, providing analytical access to the entanglement structure and nonequilibrium dynamics beyond semiclassical treatments. Defined in a reduced Hilbert space without explicit time dependence, our model enables analytical investigation of driven-dissipative dynamics and efficient numerical simulation at substantially lower cost compared to the full model. While we focus on the two-photon resonance of fluxonium as a concrete example, the framework extends naturally to higher-order multi-photon resonances [19] and is broadly applicable across different superconducting qubit architectures.

## DRIVEN-DISSIPATIVE INTERPRETATION

An analytical treatment within the reduced model reveals MIST as a driven–dissipative nonequilibrium process. We first analyze the steady state of Eq. (6) by treating the two-photon coupling  $g_{\text{eff}}$  as a perturbation,  $\hat{H}_{\text{eff}} = \hat{H}^{(0)} + \hat{H}^{(1)}$ ,  $\hat{H}^{(1)} = g_{\text{eff}}(\hat{a}^\dagger)^2 |g\rangle\langle h| + g_{\text{eff}}^* \hat{a}^2 |h\rangle\langle g|$ . To leading order, the unperturbed Liouvillian  $\mathcal{L}_0 \hat{\rho} = -i[\hat{H}^{(0)}, \hat{\rho}] + \kappa \mathcal{D}[\hat{a}](\hat{\rho})$  admits a degenerate steady-state manifold spanned by

$$\hat{\rho}_{ss}^{(0)} = \tilde{P}_g |g\rangle\langle g| \otimes |\alpha_g\rangle\langle\alpha_g| + \tilde{P}_h |h\rangle\langle h| \otimes |\alpha_h\rangle\langle\alpha_h|, \quad (7)$$

with undetermined dressed-state populations  $\tilde{P}_g$ ,  $\tilde{P}_h$ , where  $|\alpha_{g/h}\rangle$  are coherent states conditioned on the qubit state, with amplitudes  $\alpha_{g/h} = \frac{-\varepsilon_d}{\delta_a + \chi_{g/h} - i\kappa/2}$ .

Including  $\mathcal{L}_1 \hat{\rho} = -i[\hat{H}^{(1)}, \hat{\rho}]$  as a perturbation lifts the degeneracy and sets a unique steady state. Applying adiabatic elimination under the bad cavity limit  $\kappa \gg |g_{\text{eff}}|$  [21], we obtain a rate equation

$$\dot{\tilde{P}}_g = -\gamma_g \tilde{P}_g + \gamma_h \tilde{P}_h, \quad (8)$$

where the relaxation rates  $\gamma_g$ ,  $\gamma_h$  can be analytically computed from the reduced quantum model [19]. Enforcing  $\tilde{P}_g + \tilde{P}_h = 1$ , Eq. (8) reduces to

$$\dot{\tilde{P}}_g = -\gamma(\tilde{P}_g - \tilde{P}_g^{\text{ss}}), \quad (9)$$

where  $\gamma = \gamma_g + \gamma_h$ , with  $\tilde{P}_g^{\text{ss}} = \frac{\gamma_h}{\gamma_g + \gamma_h}$ . This describes an irreversible relaxation of the system towards a unique steady-state population, governed by the competition between upward and downward two-photon transitions.

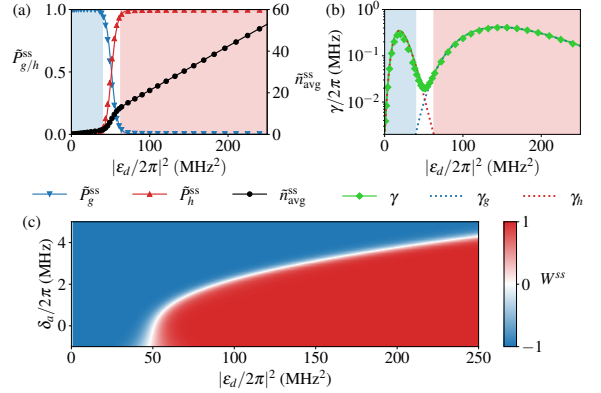


FIG. 2. (a) Steady-state qubit populations  $\tilde{P}_g^{\text{ss}}$  and  $\tilde{P}_h^{\text{ss}}$ , and average photon number  $\tilde{n}_{\text{avg}}^{\text{ss}}$  as functions of  $|\varepsilon_d|^2$ . (b) Relaxation rates  $\gamma$ ,  $\gamma_g$ , and  $\gamma_h$  as functions of  $|\varepsilon_d|^2$ . Solid/dotted lines represent analytical predictions; markers denote numerical simulations with resonator photon number cutoff up to  $n^{\text{max}} = 100$ . (c) Steady-state inversion  $W^{\text{ss}} \equiv \tilde{P}_h^{\text{ss}} - \tilde{P}_g^{\text{ss}}$  within the parameter space spanned by  $|\varepsilon_d|^2$  and  $\delta_a$ .

We identify three qualitative regimes from the steady-state population behavior shown in Fig. 2(a). Under weak drive and assuming ground-state readout, the qubit remains in the ground state and the measurement is approximately QND; this defines the **sub-MIST** regime ( $\tilde{P}_g^{\text{ss}} > 95\%$ , blue shade). As the drive increases beyond  $\varepsilon_d/2\pi \sim 6$  MHz, population begins to redistribute between  $|g\rangle$  and  $|h\rangle$ , marking the onset of **MIST** (white window). At stronger drive above  $\varepsilon_d/2\pi \sim 8$  MHz, the system enters the **super-MIST** regime ( $\tilde{P}_h^{\text{ss}} > 95\%$ , red shade), characterized by a predominantly inverted qubit. The steady-state photon number in dressed-basis  $\tilde{n}_{\text{avg}}^{\text{ss}}$  also exhibits qualitative distinctions across the three regimes: it increases approximately linearly with  $|\varepsilon_d|^2$  in the sub-MIST regime, rises sharply during the MIST window, and continues to grow linearly in the super-MIST regime with a larger slope.

The three steady-state regimes are further elucidated by the relaxation rates shown in Fig. 2(b). In the sub-MIST regime, photon loss dominates over drive-induced excitation, leading to a dominant  $\gamma_h$  that favors relaxation into  $|g, \alpha_g\rangle$ , as typical in dispersive readout. In the MIST window,  $\gamma_g$  and  $\gamma_h$  become comparable, re-

sulting in population distributed between  $|g\rangle$  and  $|h\rangle$ . In the super-MIST regime, strong driving suppresses  $\gamma_h$  and enhances  $\gamma_g$ , yielding an inverted qubit steady state. The total relaxation rate  $\gamma$  exhibits a non-monotonic dependence on  $\varepsilon_d$ . It reaches a local minimum within the MIST window and decreases again in the deep super-MIST regime, reflecting the suppression of system relaxation under strong driving conditions. The three-regime structure further extends into the parameter space defined by the drive amplitude and detuning, as evidenced by the steady-state qubit inversion in Fig. 2(c).

These observations show that the steady-state population is governed by the balance between upward and downward two-photon transitions, highlighting the nonequilibrium nature of the driven-dissipative dynamics underlying MIST. They also suggest that the drive amplitude  $\varepsilon_d$ , rather than the resonator photon number used in previous studies, is the more natural control parameter governing the onset and structure of MIST. Our driven-dissipative interpretation is further supported by excellent agreement between analytic predictions and numerical simulations using QuTiP [22], as shown in Fig. 2.

## BEYOND SEMICLASSICAL PREDICTIONS

The super-MIST regime exhibits dynamics beyond previous semiclassical analyses, which instead predict suppression of the transition probability under strong drive due to the diabatic passage within the Landau-Zener framework [9, 14, 15]. To examine this discrepancy, we perform numerical simulations comparing the reduced quantum model, the semiclassical model with backaction [9], and the full quantum model [15] as a benchmark. Starting from the system ground state, we analyze both the time evolution under a fixed strong drive and the finite-time response over a range of drive strengths.

Figure 3(a) shows the simulated dynamics under strong drive ( $\varepsilon_d/2\pi = 12$  MHz). Our reduced model faithfully reproduces the behavior of the full quantum model, including the transition to  $|h\rangle$ , supporting the emergence of the super-MIST regime. In contrast, the semiclassical approximation predicts that the qubit remains largely in the ground state ( $\sim 90\%$  population), as expected under the Landau-Zener framework. This discrepancy can be attributed to qubit-resonator entanglement, which is fundamentally inaccessible to semiclassical descriptions. As quantified by the negativity  $E_N$  shown in Fig. 3(b) [23, 24], such entanglement emerges during the transition and underlies the breakdown of QND measurement.

Prior observations interpreted as semiclassical diabatic behavior [9] may instead reflect transient, relaxation-limited dynamics, as suggested by snapshots of simulated qubit populations across a range of drive strengths plotted in Fig. 4. At an early time  $t = 0.25$   $\mu$ s [Fig. 4(a)], the

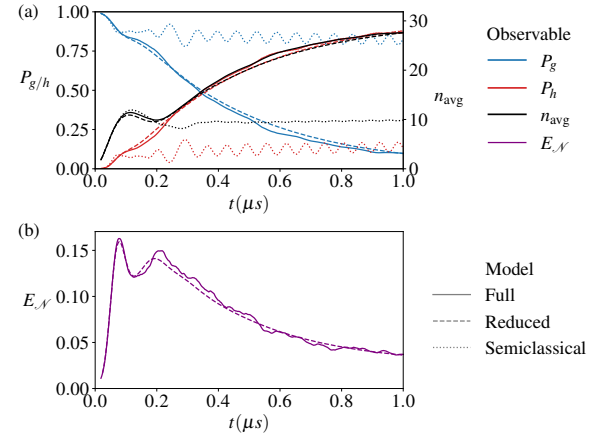


FIG. 3. (a) Time evolution of  $P_g$ ,  $P_h$ , and  $n_{avg}$  (bare-state basis) at fixed drive  $\varepsilon_d/2\pi = 12$  MHz, simulated with the full, reduced, and semiclassical models. (b) Time evolution of negativity  $E_N$ , quantifying the qubit-resonator entanglement. Simulations are performed with a qubit level cutoff at  $j^{max} = 4$  for the full and semiclassical models, and photon number cutoff up to  $n^{max} = 100$  for the full and reduced models.

semiclassical model prediction appears consistent with quantum ones. By  $t = 1 \mu$ s [Fig. 4(b)], quantitative deviations between quantum and classical predictions become apparent, although all models show a partial revival of ground-state population under strong drives, reminiscent of Landau-Zener behavior. At  $t = 5 \mu$ s [Fig. 4(c)], both quantum models show clear escape from the ground state under strong drives, while the semiclassical result remains frozen. These results indicate that what appears as diabatic protection in semiclassical models may in fact arise from slow relaxation of quantum transitions.

We further identify an underexplored short-time readout condition at high drive strengths within the super-MIST regime, where the qubit remains near its ground state ( $> 95\%$ ) while the resonator becomes highly populated, as highlighted in the green region of Fig. 4(d). This regime lies beyond semiclassical predictions, which associate strong drive with diabatic suppression of transitions and limited resonator excitation ( $n_{avg} \lesssim 15$ ). Our reduced quantum model attributes this transient protection to slowed thermalization under driven-dissipative dynamics and reveals a regime compatible with fast, high-fidelity dispersive measurement.

## CONCLUSION

In summary, we have presented a driven-dissipative interpretation of measurement-induced state transitions based on a reduced quantum model, broadly applicable across different qubit types and multi-photon resonances. The model reveals dynamics beyond semiclassical reach,

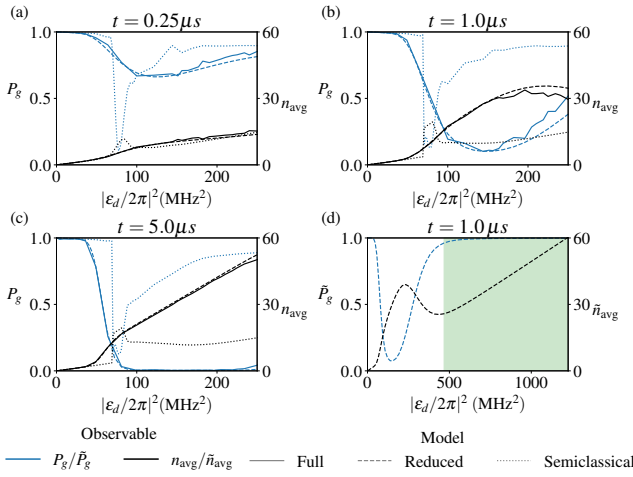


FIG. 4. Qubit ground state population and average photon number across varying drive strengths at different evolution times. (a–c) Simulated snapshots at  $t = 0.25, 1.0$ , and  $5.0 \mu\text{s}$  compare the full, reduced, and semiclassical models. Simulations use a qubit level cutoff  $j^{\max} = 4$  (full and semiclassical) and photon number cutoff up to  $n^{\max} = 100$  (full and reduced). (d) Analytical prediction from the reduced model at  $t = 1 \mu\text{s}$  in the high-drive regime.

identifies a super-MIST regime with steady-state inversion and slow relaxation, and uncovers a transient regime enabling fast, high-fidelity readout. These results establish an efficient framework for optimizing measurement protocols in strongly driven superconducting systems, grounded in the nonequilibrium dynamics underlying the breakdown of QND measurement.

Looking ahead, our work opens directions for studying critical behavior in multi-qubit or strongly coupled systems, such as multi-photon Jaynes–Cummings models [25, 26], and for examining the three-regime structure under higher-order resonances. Future experimental validation and theoretical extensions, including parasitic transitions [13] and material-induced decoherence [8], will help demonstrate the predictive power of this driven-dissipative interpretation across broader parameter regimes and extend its applicability.

We thank Huan-Hsuan Kung for helpful discussions. C.-H. Wang acknowledges funding support from the National Science and Technology Council, Taiwan, under grant numbers 111-2112-M-002-049-MY3, 114-2119-M-007-013-, 114-2124-M-002-003-, and 114-2112-M-002-021-MY3, and from the Office of Research and Development, National Taiwan University, under grant number 114L895001. C.-H. Wang is also grateful for support from the Fubon Foundation and from the Physics Division, National Center for Theoretical Sciences, Taiwan.

- [1] P. Krantz, M. Kjaergaard, F. Yan, T. P. Orlando, S. Gustavsson, and W. D. Oliver, *Applied Physics Reviews* **6**, 021318 (2019).
- [2] M. Kjaergaard, M. E. Schwartz, J. Braumüller, P. Krantz, J. I.-J. Wang, S. Gustavsson, and W. D. Oliver, *Annu. Rev. Condens. Matter Phys.* **11**, 369 (2020).
- [3] A. Blais, A. L. Grimsmo, S. M. Girvin, and A. Wallraff, *Rev. Mod. Phys.* **93**, 025005 (2021).
- [4] A. Blais, R.-S. Huang, A. Wallraff, S. M. Girvin, and R. J. Schoelkopf, *Phys. Rev. A* **69**, 062320 (2004).
- [5] A. Wallraff, D. I. Schuster, A. Blais, L. Frunzio, J. Majer, M. H. Devoret, S. M. Girvin, and R. J. Schoelkopf, *Phys. Rev. Lett.* **95**, 060501 (2005).
- [6] D. Sank, Z. Chen, M. Khezri, J. Kelly, R. Barends, *et al.*, *Phys. Rev. Lett.* **117**, 190503 (2016).
- [7] R. Lescanne, L. Verney, Q. Ficheux, M. H. Devoret, B. Huard, M. Mirrahimi, and Z. Leghtas, *Phys. Rev. Appl.* **11**, 014030 (2019).
- [8] A. Bista, M. Thibodeau, K. Nie, K. Chow, B. K. Clark, and A. Kou, [arXiv:2501.17807](https://arxiv.org/abs/2501.17807).
- [9] Z. Wang, B. D’Anjou, P. Gigan, A. Blais, and M. S. Blok, [arXiv:2505.00639](https://arxiv.org/abs/2505.00639).
- [10] M. Féchant, M. F. Dumas, D. Bénâtre, N. Gosling, P. Lenhard, M. Spiecker, W. Wernsdorfer, B. D’Anjou, A. Blais, and I. M. Pop, [arXiv:2505.00674](https://arxiv.org/abs/2505.00674).
- [11] M. Khezri, A. Opremcak, Z. Chen, K. C. Miao, M. McEwen, *et al.*, *Phys. Rev. Appl.* **20**, 054008 (2023).
- [12] K. N. Nesterov and I. V. Pechenezhskiy, *Phys. Rev. Appl.* **22**, 064038 (2024).
- [13] S. Singh, G. Refael, A. Clerk, and E. Rosenfeld, [arXiv:2412.14788](https://arxiv.org/abs/2412.14788).
- [14] R. Shillito, A. Petrescu, J. Cohen, J. Beall, M. Hauru, M. Ganahl, A. G. Lewis, G. Vidal, and A. Blais, *Phys. Rev. Applied* **18**, 034031 (2022).
- [15] M. F. Dumas, B. Groleau-Paré, A. McDonald, M. H. Muñoz-Arias, C. Lledó, B. D’Anjou, and A. Blais, *Phys. Rev. X* **14**, 041023 (2024).
- [16] Y. Nojiri, K. E. Honasoge, A. Marx, K. G. Fedorov, and R. Gross, [arXiv:2402.01884](https://arxiv.org/abs/2402.01884).
- [17] V. E. Manucharyan, J. Koch, L. I. Glazman, and M. H. Devoret, *Science* **326**, 113 (2009).
- [18] L. B. Nguyen, Y.-H. Lin, A. Somoroff, R. Mencia, N. Grabon, and V. E. Manucharyan, *Phys. Rev. X* **9**, 041041 (2019).
- [19] See Supplemental Material for detailed derivations..
- [20] C. J. Villas-Boas and D. Z. Rossatto, *Phys. Rev. Lett.* **122**, 123604 (2019).
- [21] J. I. Cirac, R. Blatt, P. Zoller, and W. D. Phillips, *Phys. Rev. A* **46**, 2668 (1992).
- [22] N. Lambert, E. Giguère, P. Menczel, B. Li, P. Hopf, *et al.*, [arXiv:2412.04705](https://arxiv.org/abs/2412.04705).
- [23] G. Vidal and R. F. Werner, *Phys. Rev. A* **65**, 032314 (2002).
- [24] C. Eichler, C. Lang, J. M. Fink, J. Govenius, S. Filipp, and A. Wallraff, *Phys. Rev. Lett.* **109**, 240501 (2012).
- [25] H. J. Carmichael, *Phys. Rev. X* **5**, 031028 (2015).
- [26] H.-J. Li, L.-B. Fan, S. Ma, J.-Q. Liao, and C.-C. Shu, *Phys. Rev. A* **110**, 043707 (2024).

\* chiaowang@phys.ntu.edu.tw

# Supplemental Material: Driven-Dissipative Interpretation of Measurement-Induced State Transitions Beyond Semiclassical Predictions

Bo-Syun Pan,<sup>1</sup> Yen-Hsiang Lin,<sup>2</sup> and Chiao-Hsuan Wang<sup>1,3,4,\*</sup>

<sup>1</sup>*Department of Physics and Center for Theoretical Physics,  
National Taiwan University, Taipei 106319, Taiwan*

<sup>2</sup>*Department of Physics, National Tsing Hua University, Hsinchu 30013, Taiwan*

<sup>3</sup>*Center for Quantum Science and Engineering, National Taiwan University, Taipei 106319, Taiwan*

<sup>4</sup>*Physics Division, National Center for Theoretical Sciences, Taipei 106319, Taiwan*

## A. DETAILED DERIVATIONS OF THE REDUCED QUANTUM MODEL

We derive the reduced qubit-resonator Hamiltonian under the two-photon resonance condition, starting from the Hamiltonian of the full quantum model of a superconducting qubit coupled to a classically driven readout resonator,

$$\hat{H}_{\text{full}}(t) = \hat{H}_{qr} + \hat{H}_d(t). \quad (\text{A1})$$

Note that we take  $\hbar = 1$  throughout for simplicity.

The static qubit-resonator Hamiltonian is

$$\hat{H}_{qr} = \omega_r \hat{a}^\dagger \hat{a} + \hat{H}_q + ig\hat{n}(\hat{a}^\dagger - \hat{a}), \quad (\text{A2})$$

where  $\omega_r$  is the bare resonator frequency,  $g$  is the qubit-resonator coupling strength, and  $\hat{n}$  is the qubit charge operator.

The qubit Hamiltonian reads

$$\hat{H}_q = 4E_C\hat{n}^2 + \frac{1}{2}E_L\hat{\varphi}^2 - E_J \cos(\hat{\varphi} - \varphi_{\text{ext}}), \quad (\text{A3})$$

where  $E_C$  is the charging energy,  $E_L$  is the inductive energy,  $E_J$  is the Josephson energy,  $\hat{\varphi}$  is the superconducting phase operator, and  $\varphi_{\text{ext}}$  is the externally applied flux in units of the flux quantum  $\Phi_0$ . This Hamiltonian can be diagonalized as

$$\hat{H}_q = \sum_j \omega_j |j\rangle\langle j|, \quad (\text{A4})$$

where  $\omega_j$  is the eigenfrequency of the  $j$ -th qubit eigenstate  $|j\rangle$ .

The resonator is driven by a classical field,

$$\hat{H}_d(t) = -2i\varepsilon_d(t) \sin(\omega_d t)(\hat{a}^\dagger - \hat{a}), \quad (\text{A5})$$

where  $\varepsilon_d(t)$  and  $\omega_d$  are the drive amplitude and frequency, respectively. All operators and parameters follow the definitions in the main text.

Including photon loss in the resonator, the system dynamics is governed by the master equation

$$\dot{\hat{\rho}} = -i[\hat{H}_{\text{full}}, \hat{\rho}] + \kappa \mathcal{D}[\hat{a}](\hat{\rho}), \quad (\text{A6})$$

with the Lindblad dissipator defined as  $\mathcal{D}[\hat{o}](\rho) = \hat{o}\rho\hat{o}^\dagger - \frac{1}{2}\{\hat{o}^\dagger\hat{o}, \rho\}$ , where  $\kappa$  denotes the resonator decay rate.

We assume that no qubit transition is resonant with the resonator at the single-photon level, i.e.,  $|gn_{ij}| \ll |\omega_j - \omega_i - \omega_r|$  for all  $i, j$ , where  $n_{ij} \equiv \langle i | \hat{n} | j \rangle$ . In contrast, the qubit ground state  $|g\rangle$  and an excited state  $|h\rangle$  satisfy the two-photon resonance condition  $\omega_h - \omega_g \approx 2\omega_r$ , leading to two-photon processes mediated by virtual intermediate states. To describe the dynamics within the resonant subspace, we perform a standard Schrieffer-Wolff transformation [1–3] to diagonalize the qubit-resonator Hamiltonian  $\hat{H}_{qr}$  to  $\mathcal{O}(g)$ , which captures the effective two-photon interactions generated by virtual single-photon transitions.

### A.I. General Framework of the Schrieffer–Wolff Transformation

We set up a general Schrieffer–Wolff (SW) framework for diagonalizing the qubit–resonator Hamiltonian  $\hat{H}_{qr}$  order by order in the coupling strength  $g$ . We first decompose the Hamiltonian as

$$\hat{H}_{qr} = \hat{H}_0 + \hat{V}^{(1)}, \quad (\text{A7})$$

where  $\hat{H}_0 = \hat{H}_q + \omega_r \hat{a}^\dagger \hat{a}$  is the free Hamiltonian of the uncoupled qubit and resonator, whose eigenstates define the bare-state basis, and  $\hat{V}^{(1)} = ig(\hat{a}^\dagger - \hat{a})$  is the first-order interaction term.

The SW transformation is defined as

$$\hat{H}_{qr} \rightarrow e^{\hat{S}} \hat{H}_{qr} e^{-\hat{S}}, \quad (\text{A8})$$

where the anti-Hermitian generator is expanded up to order  $\mathcal{O}(g^N)$  as  $\hat{S} = \sum_{p=1}^N \hat{S}^{(p)}$ , with each  $\hat{S}^{(p)}$  being of order  $\mathcal{O}(g^p)$ . The generator is chosen to cancel all off-diagonal terms through  $\mathcal{O}(g^N)$ , so that the transformed Hamiltonian takes the form

$$e^{\hat{S}} \hat{H}_{qr} e^{-\hat{S}} = \hat{H}_0 + \left( \sum_{p=1}^N \hat{V}^{(p)} \right)_{\text{d.}} + \hat{V}^{(N+1)} + \mathcal{O}(g^{N+2}), \quad (\text{A9})$$

where  $\hat{V}^{(p)}$  denotes the  $\mathcal{O}(g^p)$  effective interaction obtained after eliminating the off-diagonal terms up to order  $\mathcal{O}(g^{p-1})$ . For any operator  $\hat{O}$ , we denote its diagonal and off-diagonal parts by  $(\hat{O})_{\text{d.}}$  and  $(\hat{O})_{\text{o.d.}}$ , respectively.

To obtain a recursive construction for  $\hat{S}^{(p)}$  and  $\hat{V}^{(p)}$ , we use the Zassenhaus formula [4]

$$e^{t(\hat{X} + \hat{Y})} = e^{t\hat{X}} e^{t\hat{Y}} e^{-\frac{t^2}{2} [\hat{X}, \hat{Y}]} \dots, \quad (\text{A10})$$

which leads to

$$\exp \left( \hat{S}^{(N)} + \sum_{p=1}^{N-1} \hat{S}^{(p)} \right) = \exp \left( \hat{S}^{(N)} \right) \exp \left( \sum_{p=1}^{N-1} \hat{S}^{(p)} \right) (1 + \mathcal{O}(g^{N+1})), \quad (\text{A11})$$

$$e^{\hat{S}} \hat{H}_{qr} e^{-\hat{S}} = \hat{H}_0 + \sum_{p=1}^{N-1} (\hat{V}^{(p)})_{\text{d.}} + \hat{V}^{(N)} + [\hat{S}^{(N)}, \hat{H}_0] + \mathcal{O}(g^{N+1}). \quad (\text{A12})$$

To match the diagonalized form up to  $\mathcal{O}(g^N)$ , this requires that for all  $N \geq 1$ ,

$$[\hat{S}^{(N)}, \hat{H}_0] = - \left( \hat{V}^{(N)} \right)_{\text{o.d.}}. \quad (\text{A13})$$

Starting from the explicit forms of  $\hat{H}_0$  and  $\hat{V}^{(1)}$  defined above, the recursion relation in Eq. (A13) allows  $\hat{S}^{(N)}$  and  $\hat{V}^{(N+1)}$  to be constructed iteratively for all  $N \geq 1$ .

For an explicit construction, we use the normal ordered expansions

$$\hat{S}^{(p)} = \sum_{nm} \hat{S}_{nm}^{(p)} (\hat{a}^\dagger)^n \hat{a}^m, \quad \hat{V}^{(p)} = \sum_{nm} \hat{V}_{nm}^{(p)} (\hat{a}^\dagger)^n \hat{a}^m, \quad (\text{A14})$$

where  $\hat{S}_{nm}^{(p)}$  and  $\hat{V}_{nm}^{(p)}$  are operator components acting in the qubit subspace. With  $\hat{S}^{(p)}$  anti-Hermitian and  $\hat{V}^{(p)}$  Hermitian,

$$\left( \hat{S}_{nm}^{(p)} \right)^\dagger = -\hat{S}_{mn}^{(p)}, \quad \left( \hat{V}_{nm}^{(p)} \right)^\dagger = \hat{V}_{mn}^{(p)}. \quad (\text{A15})$$

Combining Eqs. (A14) and (A13), the coefficients of  $\hat{S}^{(p)}$  for a given order  $p$  are

$$\langle i | \hat{S}_{nm}^{(p)} | j \rangle = -\frac{\langle i | (\hat{V}_{nm}^{(p)})_{\text{o.d.}} | j \rangle}{(\omega_{ij} - \omega_r(n-m))} = -\frac{\langle i | \hat{V}_{nm}^{(p)} | j \rangle}{(\omega_{ij} - \omega_r(n-m))} (1 - \delta_{ij} \delta_{nm}), \quad (\text{A16})$$

where  $\delta_{ij}$  is the Kronecker delta symbol, and  $\omega_{ij} = \omega_j - \omega_i$  denotes the frequency difference between qubit eigenstates  $|i\rangle$  and  $|j\rangle$ . Note that  $\hat{V}^{(p)}$  is provided by the  $(p-1)$ -th order results. This offers a recursive procedure for constructing  $\hat{S}$  and the effective interactions order by order.

### A.II. Two-Photon Resonance Case

To obtain the effective two-photon interaction, we perform the first-order SW transformation, which generates the effective Hamiltonian up to second order in  $g$ . From the first-order interaction  $\hat{V}^{(1)} = ig\hat{n}(\hat{a}^\dagger - \hat{a})$ , the corresponding first-order generator reads

$$\hat{S}^{(1)} = \hat{S}_{10}^{(1)}\hat{a}^\dagger + \hat{S}_{01}^{(1)}\hat{a}, \quad \langle i | \hat{S}_{10}^{(1)} | j \rangle = -\frac{ign_{ij}}{(\omega_{ij} - \omega_r)}, \quad \hat{S}_{01}^{(1)} = -\hat{S}_{10}^{(1)}. \quad (\text{A17})$$

The second-order effective interaction  $\hat{V}^{(2)}$  then follows as

$$\begin{aligned} \hat{V}^{(2)} &= \frac{1}{2}[\hat{S}^{(1)}, [\hat{S}^{(1)}, \hat{H}_0]] + [\hat{S}^{(1)}, \hat{V}^{(1)}] = \frac{1}{2}[\hat{S}^{(1)}, \hat{V}^{(1)}] \\ &= \hat{V}_{11}^{(2)}\hat{a}^\dagger\hat{a} + \hat{V}_{00}^{(2)} + \hat{V}_{20}^{(2)}(\hat{a}^\dagger)^2 + \hat{V}_{02}^{(2)}\hat{a}^2, \end{aligned} \quad (\text{A18})$$

with the explicit forms

$$\hat{V}_{11}^{(2)} = \frac{1}{2} \left( [\hat{S}_{10}^{(1)}, \hat{V}_{01}^{(1)}] + [\hat{S}_{01}^{(1)}, \hat{V}_{10}^{(1)}] \right) = g^2 \sum_{i,j,k=0}^{\infty} |i\rangle\langle j| n_{ik} n_{kj} \left( \frac{\omega_{ki}}{\omega_{ki}^2 - \omega_r^2} + \frac{\omega_{kj}}{\omega_{kj}^2 - \omega_r^2} \right), \quad (\text{A19})$$

$$\hat{V}_{00}^{(2)} = \frac{1}{2} \left( \hat{S}_{01}^{(1)}\hat{V}_{10}^{(1)} - \hat{S}_{10}^{(1)}\hat{V}_{01}^{(1)} \right) = \frac{g^2}{2} \sum_{i,j,k=0}^{\infty} |i\rangle\langle j| n_{ik} n_{kj} \left( \frac{1}{\omega_{ki} - \omega_r} + \frac{1}{\omega_{kj} - \omega_r} \right), \quad (\text{A20})$$

$$\hat{V}_{20}^{(2)} = \frac{1}{2}[\hat{S}_{10}^{(1)}, \hat{V}_{10}^{(1)}] = \frac{g^2}{2} \sum_{i,j,k=0}^{\infty} |i\rangle\langle j| n_{ik} n_{kj} \left( \frac{1}{\omega_{ik} - \omega_r} - \frac{1}{\omega_{kj} - \omega_r} \right), \quad (\text{A21})$$

$$\hat{V}_{02}^{(2)} = (\hat{V}_{20}^{(2)})^\dagger. \quad (\text{A22})$$

The transformed Hamiltonian takes the form

$$e^{\hat{S}}\hat{H}_{qr}e^{-\hat{S}} = \hat{H}_0 + \hat{V}^{(2)} + \mathcal{O}(g^3) = \hat{H}_q + \omega_r\hat{a}^\dagger\hat{a} + \hat{V}_{11}^{(2)}\hat{a}^\dagger\hat{a} + \hat{V}_{00}^{(2)} + \hat{V}_{20}^{(2)}(\hat{a}^\dagger)^2 + (\hat{V}_{20}^{(2)})^\dagger\hat{a}^2 + \mathcal{O}(g^3). \quad (\text{A23})$$

We now restrict the qubit Hilbert space to the subspace spanned by  $|g\rangle, |h\rangle$  and apply the rotating wave approximation (RWA) to neglect non-resonant terms. For  $\hat{V}_{11}^{(2)}$  and  $\hat{V}_{00}^{(2)}$ , we retain only their diagonal components, giving state-dependent dispersive and energy shifts. For  $\hat{V}_{20}^{(2)}$ , we keep only the terms involving  $|g\rangle\langle h|$ , which describe the resonant two-photon transition. The transformed Hamiltonian under RWA is then

$$\begin{aligned} e^{\hat{S}}\hat{H}_{qr}e^{-\hat{S}} &\approx \omega_r\hat{a}^\dagger\hat{a} + (\omega_g + \Lambda_g + \chi_g\hat{a}^\dagger\hat{a})|g\rangle\langle g| + (\omega_h + \Lambda_h + \chi_h\hat{a}^\dagger\hat{a})|h\rangle\langle h| \\ &\quad + g_{\text{eff}}(\hat{a}^\dagger)^2|g\rangle\langle h| + g_{\text{eff}}^*(\hat{a})^2|h\rangle\langle g|, \end{aligned} \quad (\text{A24})$$

where  $\chi_i = \langle i | \hat{V}_{11}^{(2)} | i \rangle$  are the dispersive coupling strengths,  $\Lambda_i = \langle i | \hat{V}_{00}^{(2)} | i \rangle$  are the qubit energy shifts, and  $g_{\text{eff}} = \langle g | \hat{V}_{20}^{(2)} | h \rangle$  is the effective two-photon coupling strength.

We next apply the same SW transformation to the drive Hamiltonian under a constant amplitude  $\varepsilon_d(t) = \varepsilon_d$ ,

$$\begin{aligned} e^{\hat{S}}\hat{H}_de^{-\hat{S}} &= -2i\varepsilon_d \sin(\omega_dt)(\hat{a}^\dagger - \hat{a}) + [\hat{S}, -2i\varepsilon_d \sin(\omega_dt)(\hat{a}^\dagger - \hat{a})] + \mathcal{O}(\varepsilon_d g^2) \\ &= -2i\varepsilon_d \sin(\omega_dt)(\hat{a}^\dagger - \hat{a}) - 2i\varepsilon_d \sin(\omega_dt)(\hat{S}_{01}^{(1)} + \hat{S}_{10}^{(1)}) + \mathcal{O}(\varepsilon_d g^2). \end{aligned} \quad (\text{A25})$$

The second term evaluates to

$$-2i\varepsilon_d \sin(\omega_dt)(\hat{S}_{01}^{(1)} + \hat{S}_{10}^{(1)}) = i\varepsilon_d(e^{i\omega_dt} - e^{-i\omega_dt}) \left( \sum_{i,j} \frac{gn_{ij}}{\omega_{ij} - \omega_r} |i\rangle\langle j| + \text{H.C.} \right). \quad (\text{A26})$$

For a near-resonant drive  $\omega_d \approx \omega_r$ , with  $|\omega_{ij} - \omega_d|$  remaining large for all qubit states, the terms in Eq. (A26) are off-resonant and can be neglected provided

$$|\varepsilon_d g n_{ij}| \ll |(\omega_{ij} - \omega_r)(\omega_{ij} \pm \omega_d)|. \quad (\text{A27})$$

Under the RWA, the second term in Eq. (A25) is dropped and the first term simplifies to

$$e^{\hat{S}} \hat{H}_d e^{-\hat{S}} \approx \varepsilon_d \hat{a}^\dagger e^{i\omega_d t} + \varepsilon_d \hat{a} e^{-i\omega_d t}. \quad (\text{A28})$$

Finally, we apply the SW transformation to the Lindblad dissipator,

$$\kappa \mathcal{D}[\hat{a}](\hat{\rho}) \rightarrow \kappa \mathcal{D}[e^{\hat{S}} \hat{a} e^{-\hat{S}}](\hat{\rho}) = \kappa \mathcal{D}[\hat{a}](\hat{\rho}) - \frac{\kappa}{2} \left\{ \left( 2\hat{S}_{10}^{(1)} \hat{\rho} \hat{a}^\dagger - \hat{a}^\dagger \hat{S}_{10}^{(1)} \hat{\rho} - \hat{\rho} \hat{a}^\dagger \hat{S}_{10}^{(1)} \right) + \text{H.C.} \right\} + \mathcal{O}(\kappa g^2). \quad (\text{A29})$$

Note that the density operator after the transformation is in the dressed-state basis. To estimate the first-order correction, we move to the rotating frame  $\hat{U}(t) = \exp[-i(\hat{H}_q + \omega_d \hat{a}^\dagger \hat{a})t]$ ,  $\omega_d \approx \omega_r$  under which the operator  $\hat{S}_{10}^{(1)} \hat{a}^\dagger$  acquires fast oscillating phases  $e^{-i(\omega_j - \omega_i - \omega_d)t}$ . Since all detunings  $|\omega_{ij} - \omega_r|$  are assumed large, the correction is suppressed and can be neglected when

$$|\kappa g n_{ij}| \ll (\omega_{ij} - \omega_r)^2. \quad (\text{A30})$$

Collecting all terms under the RWA, the Hamiltonian in the reduced subspace,  $\hat{H}_{\text{red}} = e^{\hat{S}} \hat{H}_{\text{full}} e^{-\hat{S}}$ , and the corresponding Lindblad master equation read

$$\hat{H}_{\text{red}} \approx \omega_r \hat{a}^\dagger \hat{a} + (\omega_g + \Lambda_g + \chi_g \hat{a}^\dagger \hat{a}) |g\rangle\langle g| + (\omega_h + \Lambda_h + \chi_h \hat{a}^\dagger \hat{a}) |h\rangle\langle h| + g_{\text{eff}}(\hat{a}^\dagger)^2 |g\rangle\langle h| + g_{\text{eff}}^*(\hat{a})^2 |h\rangle\langle g| + \varepsilon_d (\hat{a}^\dagger e^{i\omega_d t} + \hat{a} e^{-i\omega_d t}), \quad (\text{A31})$$

$$\dot{\hat{\rho}} = -i[\hat{H}_{\text{red}}, \hat{\rho}] + \kappa \mathcal{D}[\hat{a}](\hat{\rho}). \quad (\text{A32})$$

Moving to the rotating frame  $\hat{U}_r(t) = \exp[-i(\omega_d \hat{a}^\dagger \hat{a} + 2\omega_d |h\rangle\langle h|)t]$ , we arrive at the effective Hamiltonian and the corresponding master equation presented in the main text,

$$\hat{H}_{\text{eff}} = \delta_a \hat{a}^\dagger \hat{a} + (\delta_g + \chi_g \hat{a}^\dagger \hat{a}) |g\rangle\langle g| + (\delta_h + \chi_h \hat{a}^\dagger \hat{a}) |h\rangle\langle h| + g_{\text{eff}}(\hat{a}^\dagger)^2 |g\rangle\langle h| + g_{\text{eff}}^*(\hat{a})^2 |h\rangle\langle g| + \varepsilon_d (\hat{a}^\dagger + \hat{a}), \quad (\text{A33})$$

$$\dot{\hat{\rho}} = -i[\hat{H}_{\text{eff}}, \hat{\rho}] + \kappa \mathcal{D}[\hat{a}](\hat{\rho}), \quad (\text{A34})$$

where  $\delta_a = \omega_r - \omega_d$ ,  $\delta_g = \omega_g + \Lambda_g$ ,  $\delta_h = \omega_h + \Lambda_h - 2\omega_d$ .

### A.III. Extension to Higher-Order Resonances: Three-Photon Example

As an illustration of higher-order processes, we present the extension of the SW transformation to the third order. The effective interaction at  $\mathcal{O}(g^3)$  is

$$\begin{aligned} \hat{V}^{(3)} &= [\hat{S}^{(2)}, \hat{V}^{(1)}] + \frac{1}{2!} \left( [\hat{S}^{(2)}, [\hat{S}^{(1)}, \hat{H}_0]] + [\hat{S}^{(1)}, [\hat{S}^{(1)}, \hat{V}^{(1)}]] + [\hat{S}^{(1)}, [\hat{S}^{(2)}, \hat{H}_0]] \right) \\ &\quad + \frac{1}{3!} \left( [\hat{S}^{(1)}, [\hat{S}^{(1)}, [\hat{S}^{(1)}, \hat{H}_0]]] \right) \\ &= \frac{1}{2} [\hat{S}^{(2)}, \hat{V}^{(1)}] - \frac{1}{6} [\hat{S}^{(1)}, \hat{V}^{(2)}] + \frac{1}{2} [\hat{S}^{(1)}, (\hat{V}^{(2)})_{\text{d}}]. \end{aligned} \quad (\text{A35})$$

By substituting the solution of the generator  $\hat{S}^{(p)}$  from Eq. (A16) into the expression for  $\hat{V}^{(3)}$  in Eq. (A35), the non-zero elements of  $\hat{V}^{(3)}$  can be expressed in terms of lower-order contributions of  $\hat{V}$  and  $\hat{S}$ :

$$\begin{aligned} \hat{V}_{10}^{(3)} &= \frac{1}{2} \left( \hat{S}_{11}^{(2)} \hat{V}_{10}^{(1)} + [\hat{S}_{00}^{(2)}, \hat{V}_{10}^{(1)}] - 2\hat{V}_{01}^{(1)} \hat{S}_{20}^{(2)} \right) - \frac{1}{6} \left( \hat{V}_{11}^{(2)} \hat{S}_{10}^{(1)} + [\hat{S}_{10}^{(1)}, \hat{V}_{00}^{(2)}] + 2\hat{S}_{01}^{(1)} \hat{V}_{20}^{(2)} \right) \\ &\quad + \frac{1}{2} \left( (\hat{V}_{11}^{(2)})_{\text{d}} \hat{S}_{10}^{(1)} + [\hat{S}_{10}^{(1)}, (\hat{V}_{00}^{(2)})_{\text{d}}] \right), \end{aligned} \quad (\text{A36})$$

$$\hat{V}_{21}^{(3)} = \frac{1}{2} \left( [\hat{S}_{11}^{(2)}, \hat{V}_{10}^{(1)}] + [\hat{S}_{20}^{(2)}, \hat{V}_{01}^{(1)}] \right) - \frac{1}{6} \left( [\hat{S}_{10}^{(1)}, \hat{V}_{11}^{(2)}] + [\hat{S}_{01}^{(1)}, \hat{V}_{02}^{(2)}] \right) + \frac{1}{2} \left( [\hat{S}_{10}^{(1)}, (\hat{V}_{11}^{(2)})_{\text{d}}] \right), \quad (\text{A37})$$

$$\hat{V}_{30}^{(3)} = \frac{1}{2} [\hat{S}_{20}^{(2)}, \hat{V}_{10}^{(1)}] - \frac{1}{6} [\hat{S}_{10}^{(1)}, \hat{V}_{02}^{(2)}], \quad (\text{A38})$$

$$\hat{V}_{01}^{(3)} = (\hat{V}_{10}^{(3)})^\dagger, \quad \hat{V}_{12}^{(3)} = (\hat{V}_{21}^{(3)})^\dagger, \quad \hat{V}_{03}^{(3)} = (\hat{V}_{30}^{(3)})^\dagger. \quad (\text{A39})$$

For a three-photon resonance between the qubit ground state  $|g\rangle$  and an excited state  $|j\rangle$ , with no lower-order resonances, the reduced Hamiltonian after RWA is

$$e^{\hat{S}} \hat{H}_{qr} e^{-\hat{S}} \approx \hat{H}_q + \omega_r \hat{a}^\dagger \hat{a} + (\omega_g + \Lambda_g + \chi_g \hat{a}^\dagger \hat{a}) |g\rangle\langle g| + (\omega_j + \Lambda_j + \chi_j \hat{a}^\dagger \hat{a}) |j\rangle\langle j| + g_{\text{eff}}^{(3)} (\hat{a}^\dagger)^3 |g\rangle\langle j| + (g_{\text{eff}}^{(3)})^* (\hat{a})^3 |j\rangle\langle g|, \quad (\text{A40})$$

where  $g_{\text{eff}}^{(3)} = \langle g | \hat{V}_{30}^{(3)} | j \rangle$ . The matrix elements of  $\hat{V}_{30}^{(3)}$  are

$$\langle i | \hat{V}_{30}^{(3)} | j \rangle = \sum_{k\ell} i g^3 n_{i\ell} n_{\ell k} n_{kj} \left\{ - \left( \frac{1}{2} \frac{1}{\omega_{ki} - 2\omega_r} + \frac{1}{6} \frac{1}{\omega_{kj} - \omega_r} \right) \left( \frac{1}{\omega_{i\ell} - \omega_r} - \frac{1}{\omega_{kj} - \omega_r} \right) \right. \\ \left. + \left( \frac{1}{2} \frac{1}{\omega_{\ell j} - 2\omega_r} + \frac{1}{6} \frac{1}{\omega_{i\ell} - \omega_r} \right) \left( \frac{1}{\omega_{\ell k} - \omega_r} - \frac{1}{\omega_{kj} - \omega_r} \right) \right\}. \quad (\text{A41})$$

The same procedure generalizes to  $k$ -photon resonances, yielding effective couplings  $g_{\text{eff}}^{(k)}$  through SW transformation and subsequent RWA.

## B. DRIVEN-DISSIPATIVE ANALYSIS OF THE REDUCED QUANTUM MODEL

We consider the Hamiltonian in the reduced subspace, where the qubit states are spanned by  $|g\rangle, |h\rangle$ . The corresponding Pauli operators are defined as

$$\hat{\sigma}_z = |h\rangle\langle h| - |g\rangle\langle g|, \quad \hat{\sigma}_+ = |h\rangle\langle g|, \quad \hat{\sigma}_- = |g\rangle\langle h|. \quad (\text{B1})$$

Treating  $g_{\text{eff}}$  as a small parameter, the Hamiltonian in Eq. (A33) can be expanded to the zeroth and first order in  $g_{\text{eff}}$  as

$$\hat{H}_{\text{eff}} = \hat{H}^{(0)} + \hat{H}^{(1)}, \quad (\text{B2})$$

where

$$\hat{H}^{(0)} = \hat{\chi} \hat{a}^\dagger \hat{a} + \frac{1}{2} \delta_q \hat{\sigma}_z + \varepsilon_d \hat{a}^\dagger + \varepsilon_d^* \hat{a} + \delta_h + \delta_g \quad (\text{B3})$$

$$\hat{H}^{(1)} = g_{\text{eff}} (\hat{a}^\dagger)^2 \hat{\sigma}_- + g_{\text{eff}}^* \hat{a}^2 \hat{\sigma}_+. \quad (\text{B4})$$

Here  $\hat{\chi} = \chi_g |g\rangle\langle g| + \chi_f |h\rangle\langle h|$ ,  $\chi_i = \chi_{i_g} + \omega_r - \omega_d$ ,  $\delta_q = \delta_h - \delta_g$ . Note that  $\chi_i$  is redefined from Eq. (A33) by absorbing the resonator detuning for compactness, which introduces an overall energy shift  $\delta_h + \delta_g$  that can be safely discarded in the subsequent analysis. After including resonator relaxation, we will first determine the steady-state solution of the zeroth-order Hamiltonian, and then treat the two-photon resonance term as a perturbation to obtain the final steady state and the corresponding driven-dissipative dynamics.

### B.I. Zeroth-Order Steady States without Two-Photon Resonance

We first solve the Lindblad master equation for the zeroth-order Hamiltonian  $\hat{H}^{(0)}$ :

$$\mathcal{L}_0 \hat{\rho} = -i[\hat{H}^{(0)}, \hat{\rho}] + \kappa \mathcal{D}[\hat{a}^\dagger] \hat{\rho} = -i(\hat{H}_{\text{NH}} \hat{\rho} - \hat{\rho} \hat{H}_{\text{NH}}) + \kappa \hat{a} \hat{\rho} \hat{a}^\dagger, \quad (\text{B5})$$

where the non-Hermitian Hamiltonian is defined as  $\hat{H}_{\text{NH}} = \hat{H} - \frac{i\kappa}{2} \hat{a}^\dagger \hat{a}$ .

To eliminate the drive term in  $\hat{H}_{\text{NH}}$ , we move to a conditional displaced frame by defining

$$\hat{D}_c = \exp(\hat{\alpha} \hat{a}^\dagger - \hat{\alpha}^\dagger \hat{a}), \quad (\text{B6})$$

$$\hat{\alpha} \equiv \alpha_h |h\rangle\langle h| + \alpha_g |g\rangle\langle g|, \quad (\text{B7})$$

with the commutation relations  $[\hat{a}^\dagger, \hat{\alpha}] = [\hat{\sigma}_z, \hat{\alpha}] = 0$ . Under the conditional displacement transformation,

$$\hat{D}_c^\dagger \hat{a} \hat{D}_c = \hat{a} + \hat{\alpha}, \quad \hat{D}_c^\dagger \hat{\sigma}_z \hat{D}_c = \hat{\sigma}_z. \quad (\text{B8})$$

The master equation in the transformed frame becomes

$$\check{\rho} = \check{\mathcal{L}}_0 \check{\rho} = -i(\check{H}_{\text{NH}} \check{\rho} - \check{\rho} \check{H}_{\text{NH}}^\dagger) + \kappa(\hat{a} + \hat{\alpha})\check{\rho}(\hat{a}^\dagger + \hat{\alpha}^\dagger), \quad (\text{B9})$$

where  $\check{\rho} = \hat{D}_c^\dagger \hat{\rho} \hat{D}_c$  and the transformed non-Hermitian Hamiltonian is

$$\check{H}_{\text{NH}} = \hat{D}_c^\dagger \hat{H}_{\text{NH}} \hat{D}_c \\ = (\hat{\chi} - \frac{i\kappa}{2})\hat{a}^\dagger \hat{a} + \left( (\hat{\chi} - \frac{i\kappa}{2})\hat{a}^\dagger \hat{\alpha} + \varepsilon_d \hat{a}^\dagger \right) + \left( (\hat{\chi} - \frac{i\kappa}{2})\hat{a} \hat{\alpha}^\dagger + \varepsilon_d^* \hat{a} \right) + (\hat{\chi} - \frac{i\kappa}{2})\hat{a}^\dagger \hat{\alpha} + \frac{1}{2}\delta_q \hat{\sigma}_z + \varepsilon_d \hat{a}^\dagger + \varepsilon_d^* \hat{a}. \quad (\text{B10})$$

Choosing  $\alpha_g = \frac{-\varepsilon_d}{\check{\chi}_g - i\kappa/2}$  and  $\alpha_h = \frac{-\varepsilon_d}{\check{\chi}_h - i\kappa/2}$  such that  $\hat{\alpha} = -\frac{\varepsilon_d}{\check{\chi} - i\kappa/2}$  eliminates the linear drive term from the transformed non-Hermitian Hamiltonian, yielding

$$\hat{H}_{\text{NH}} = (\hat{\chi} - \frac{i\kappa}{2})\hat{a}^\dagger \hat{a} - i\kappa \hat{\alpha}^\dagger \hat{a} - \frac{i\kappa}{2}\hat{a}^\dagger \hat{\alpha} + \frac{1}{2}\check{\delta}_q \hat{\sigma}_z + C, \quad (\text{B11})$$

where

$$\check{\delta}_q = \delta_q + \check{\chi}_h |\alpha_h|^2 - \check{\chi}_g |\alpha_g|^2 + \varepsilon_d (\alpha_h^* - \alpha_g^*) + \varepsilon_d^* (\alpha_h - \alpha_g), \quad (\text{B12})$$

$$C = \frac{1}{2} (\check{\chi}_h |\alpha_h|^2 + \check{\chi}_g |\alpha_g|^2 + \varepsilon_d (\alpha_h^* + \alpha_g^*) + \varepsilon_d^* (\alpha_h + \alpha_g)). \quad (\text{B13})$$

The zeroth-order master equation in the transformed frame now reads

$$\check{\mathcal{L}}_0 \check{\rho} = -i[\hat{\chi} \hat{a}^\dagger \hat{a} + \frac{1}{2}\delta_q \hat{\sigma}_z, \check{\rho}] + \kappa \mathcal{D}[\hat{a}] \check{\rho} + \kappa \hat{a}[\check{\rho}, \hat{a}^\dagger] + \kappa [\hat{\alpha}, \check{\rho}] \hat{a}^\dagger + \kappa \mathcal{D}[\hat{\alpha}] \check{\rho}, \quad (\text{B14})$$

which admits the steady-state solution

$$\check{\rho}_{ss}^{(0)} = \left( \tilde{P}_g |g\rangle\langle g| + \tilde{P}_h |h\rangle\langle h| \right) \otimes |0\rangle\langle 0|, \quad (\text{B15})$$

with arbitrary  $\tilde{P}_g, \tilde{P}_h > 0$  satisfying  $\tilde{P}_g + \tilde{P}_h = 1$ , showing a two-fold degeneracy in the qubit subspace. Moving back to the non-displaced frame, the zeroth-order steady state takes the form

$$\check{\rho}_{ss}^{(0)} = \hat{D}_c \check{\rho}_{ss}^{(0)} \hat{D}_c^\dagger = \tilde{P}_g |g\rangle\langle g| \otimes |\alpha_g\rangle\langle\alpha_g| + \tilde{P}_h |h\rangle\langle h| \otimes |\alpha_h\rangle\langle\alpha_h|, \quad (\text{B16})$$

where  $|\alpha_{g/h}\rangle$  are coherent states with amplitudes  $\alpha_{g/h}$ .

## B.II. Unique Steady State and Relaxation Rates under Two-Photon Resonance

Building on the zeroth-order analysis in Sec. B.I,  $\check{\mathcal{L}}_0$  drives the system into the degenerate steady-state manifold on the fast timescale set by  $1/\kappa$ . We now include the two-photon transition term  $H^{(1)}$  as a perturbation to the dynamics on slower timescales. Since the rapid zeroth-order relaxation keeps the state confined to this manifold, we take  $\check{\rho}^{(0)}$  to be the steady-state solution of Sec. B.I throughout the perturbative expansion,

$$\check{\rho}^{(0)} = \left( \tilde{P}_g |g\rangle\langle g| + \tilde{P}_h |h\rangle\langle h| \right) \otimes |0\rangle\langle 0|. \quad (\text{B17})$$

The full Liouvillian in the transformed frame is

$$\dot{\check{\rho}} = \check{\mathcal{L}}_0 \check{\rho} + \check{\mathcal{L}}_1 \check{\rho}, \quad (\text{B18})$$

where  $\check{\mathcal{L}}_0$  is defined in Eq. (B14) and the first-order Liouvillian is given by

$$\check{\mathcal{L}}_1 \check{\rho} = -i[\check{H}^{(1)}, \check{\rho}], \quad (\text{B19})$$

$$\check{H}^{(1)} = \hat{D}_c^\dagger \hat{H}^{(1)} \hat{D}_c = g_{\text{eff}} (\hat{A}^{(2)})^\dagger \hat{\sigma}_- + \text{H.C.}, \quad (\text{B20})$$

$$\hat{A}^{(k)} \equiv \hat{D}^\dagger(\alpha_h) \hat{a}^k \hat{D}(\alpha_g). \quad (\text{B21})$$

The total density matrix can be expressed in the two-level qubit subspace as

$$\check{\rho} = \check{\rho}_{gg} |g\rangle\langle g| + \check{\rho}_{hh} |h\rangle\langle h| + \check{\rho}_{hg} |h\rangle\langle g| + \check{\rho}_{gh} |g\rangle\langle h|, \quad (\text{B22})$$

where each  $\check{\rho}_{ij}$  is an operator acting on the resonator Hilbert space, and  $\check{\rho}_{hg} = \check{\rho}_{gh}^\dagger$  ensures the Hermiticity of the density matrix.

To proceed, we carry out a perturbative expansion of the dynamics order by order. We start with the first-order correction by expanding the density matrix as  $\check{\rho} \approx \check{\rho}^{(0)} + \check{\rho}^{(1)}$ , where  $\check{\rho}^{(0)}$  is block-diagonal in the qubit basis and belongs to the degenerate steady-state manifold given in Eq. (B17). In this structure, the off-diagonal elements  $\check{\rho}_{hg}$  and  $\check{\rho}_{gh}$  vanish at the zeroth order and are generated only through the coupling induced by  $\check{\mathcal{L}}_1$ . Under the limit  $|g_{\text{eff}}| \ll \kappa$ , the zeroth-order relaxation driven by  $\check{\mathcal{L}}_0$  occurs on a timescale much shorter than the two-photon transition, allowing us to adiabatically eliminate  $\check{\rho}_{hg}$  by setting  $\dot{\check{\rho}}_{hg} = \dot{\check{\rho}}_{gh}^\dagger \approx 0$ .

Setting  $\dot{\check{\rho}}_{hg} = 0$ , the off-diagonal term adiabatically follows the block-diagonal populations, satisfying

$$\dot{\check{\rho}}_{hg}^{(1)} = \left( \check{\mathcal{L}}_0 \check{\rho}^{(1)} \right)_{hg} + \left( \check{\mathcal{L}}_1 \check{\rho}^{(0)} \right)_{hg} = 0 \Rightarrow \check{\mathcal{L}}_0 \left( \check{\rho}_{hg}^{(1)} \hat{\sigma}_+ \right) + \left( \check{\mathcal{L}}_1 \check{\rho}^{(0)} \right)_{hg} \hat{\sigma}_+ = 0. \quad (\text{B23})$$

Expanding  $\check{\rho}_{hg} = \check{\rho}_{hg}^{(1)}$  in the resonator Fock basis,  $\check{\rho}_{hg} = \sum_{nm} \rho_{hg}^{nm} |n\rangle\langle m|$ , we obtain

$$\begin{aligned} \check{\mathcal{L}}_0 \left( \check{\rho}_{hg}^{(1)} \hat{\sigma}_+ \right) &= \sum_{nm} |n\rangle\langle m| \hat{\sigma}_+ \left( c_{nm}^{00} \rho_{hg}^{nm} + c_{nm}^{10} \rho_{hg}^{n+1,m} + c_{nm}^{01} \rho_{hg}^{n,m+1} + c_{nm}^{11} \rho_{hg}^{n+1,m+1} \right), \\ \left( \check{\mathcal{L}}_1 \check{\rho}^{(0)} \right)_{hg} &= -ig_{\text{eff}}^* \left( \tilde{P}_g \hat{A}^{(2)} |0\rangle\langle 0| - \tilde{P}_h |0\rangle\langle 0| \hat{A}^{(2)} \right) = -ig_{\text{eff}}^* \sum_{nm} \left( \tilde{P}_g A_{n0}^{(2)} \delta_{0m} - \tilde{P}_h A_{0m}^{(2)} \delta_{n0} \right) |n\rangle\langle m|, \end{aligned} \quad (\text{B24})$$

where the coefficients are given by

$$\begin{aligned} c_{nm}^{00} &= -i(\check{\chi}_h n - \check{\chi}_g m + \check{\delta}_q) - \frac{\kappa}{2}(n+m) + \kappa(\alpha_h \alpha_g^* - \frac{1}{2}(|\alpha_h|^2 + |\alpha_g|^2)) \\ &= \left( -i\check{\chi}_h - \frac{\kappa}{2} \right) n + \left( i\check{\chi}_g - \frac{\kappa}{2} \right) m - i(\check{\chi}_h - \check{\chi}_g) \alpha_g^* \alpha_e + \delta_q, \end{aligned} \quad (\text{B25})$$

$$c_{nm}^{10} = \kappa(\alpha_g^* - \alpha_h^*) \sqrt{n+1}, \quad (\text{B26})$$

$$c_{nm}^{01} = -\kappa(\alpha_g - \alpha_h) \sqrt{m+1}, \quad (\text{B27})$$

$$c_{nm}^{11} = \kappa \sqrt{(n+1)(m+1)}. \quad (\text{B28})$$

Substituting the Fock-basis expansions of  $\check{\mathcal{L}}_0(\check{\rho}_{hg}^{(1)} \hat{\sigma}_+)$  and  $(\check{\mathcal{L}}_1 \check{\rho}^{(0)})_{hg}$  from Eq. (B24) into Eq. (B23) yields

$$c_{nm}^{00} \rho_{hg}^{nm} + c_{nm}^{10} \rho_{hg}^{n+1,m} + c_{nm}^{01} \rho_{hg}^{n,m+1} + c_{nm}^{11} \rho_{hg}^{n+1,m+1} = ig_{\text{eff}}^* (\tilde{P}_g A_{n0}^{(2)} \delta_{0m} - \tilde{P}_h A_{0m}^{(2)} \delta_{n0}). \quad (\text{B29})$$

Because the right-hand side is nonzero only when either  $n = 0$  or  $m = 0$ , it follows that  $\rho_{hg}^{nm}$  is nonzero only in these cases. We can therefore write

$$\rho_{hg}^{nm} = ig_{\text{eff}}^* (\tilde{P}_g x_n^g \delta_{0m} - \tilde{P}_h x_m^h \delta_{n0}), \quad (\text{B30})$$

$$\check{\rho}_{hg} = ig_{\text{eff}}^* \left( \sum_{n=0}^{\infty} \tilde{P}_g x_n^g |n\rangle\langle 0| - \sum_{n=0}^{\infty} \tilde{P}_h x_n^h |0\rangle\langle n| \right), \quad (\text{B31})$$

where  $x_n^g$  and  $x_n^h$  satisfy

$$c_{n0}^{00} x_n^g + c_{n0}^{10} x_{n+1}^g = A_{n0}^{(2)}, \quad (\text{B32})$$

$$c_{0n}^{00} x_n^h + c_{0n}^{01} x_{n+1}^h = A_{0n}^{(2)}. \quad (\text{B33})$$

Both recurrence relations can be cast into the generic form  $b_n x_n + d_n x_{n+1} = y_n$ , whose formal solution is

$$x_n = \sum_{\ell=n}^{\infty} (-1)^{\ell-n} \frac{y_\ell}{b_\ell} \left( \prod_{k=n}^{\ell-1} \frac{d_k}{b_k} \right). \quad (\text{B34})$$

Applying this solution to the two specific cases, we find

$$x_n^g = \sum_{\ell=n}^{\infty} (-1)^{\ell-n} \frac{A_{\ell 0}^{(2)}}{c_{\ell 0}^{00}} \left( \prod_{k=n}^{\ell-1} \frac{c_{k0}^{10}}{c_{k0}^{00}} \right), \quad (\text{B35})$$

$$x_n^h = \sum_{\ell=n}^{\infty} (-1)^{\ell-n} \frac{A_{0\ell}^{(2)}}{c_{0\ell}^{00}} \left( \prod_{k=n}^{\ell-1} \frac{c_{0k}^{01}}{c_{0k}^{00}} \right). \quad (\text{B36})$$

Next, we extend the perturbative expansion to second order,  $\check{\rho} = \check{\rho}^{(0)} + \check{\rho}^{(1)} + \check{\rho}^{(2)}$ . The first-order correction describes how the off-diagonal elements adiabatically follow the diagonal populations. The second-order correction will capture the resulting slow population transfer between the qubit ground and excited states, which governs the non-equilibrium dynamics and determines the unique steady state. The second-order dynamics is given by

$$\dot{\check{\rho}}^{(2)} = \check{\mathcal{L}}_0(\check{\rho}^{(2)}) + \check{\mathcal{L}}_1(\check{\rho}^{(1)}). \quad (\text{B37})$$

Assume  $\kappa \gg |g_{\text{eff}}|$ , the fast dynamics of  $\check{\mathcal{L}}_0$  quickly relaxes the system into the subspace  $\{|g, 0\rangle, |h, 0\rangle\}$ . Within this subspace, the second-order dynamics reads

$$\begin{aligned} \dot{\check{\rho}}^{(2)} &\approx \sum_{i \in \{g, h\}} \text{Tr}_r \left[ |i\rangle\langle i| \check{\mathcal{L}}_1(\check{\rho}^{(1)}) |i\rangle\langle i| \right] \otimes |0\rangle\langle 0| \\ &= -ig_{\text{eff}} \text{Tr}_r \left[ (\hat{A}^{(2)})^\dagger \check{\rho}_{hg} |g\rangle\langle g| - \check{\rho}_{hg} (\hat{A}^{(2)})^\dagger |h\rangle\langle h| \right] \otimes |0\rangle\langle 0| + \text{H.c.} \\ &\equiv \left( \dot{\tilde{P}}_g |g\rangle\langle g| + \dot{\tilde{P}}_h |h\rangle\langle h| \right) \otimes |0\rangle\langle 0|, \end{aligned} \quad (\text{B38})$$

where  $\text{Tr}_r$  is the partial trace over the degrees of freedom of the resonator.

Inserting the solution of  $\check{\rho}_{hg}$  from Eq. (B31) into Eq. (B38), we obtain the closed rate equations for the qubit populations:

$$\dot{\tilde{P}}_g = -\gamma_g \tilde{P}_g + \gamma_h \tilde{P}_h, \quad \dot{\tilde{P}}_h = -\dot{\tilde{P}}_g, \quad (\text{B39})$$

where the transition rates  $\gamma_g$  and  $\gamma_h$  are given by

$$\gamma_g = -2|g_{\text{eff}}|^2 \text{Re} \left( \sum_{n=0}^{\infty} \left( A_{n0}^{(2)} \right)^* x_n^g \right), \quad (\text{B40})$$

$$\gamma_h = -2|g_{\text{eff}}|^2 \text{Re} \left( \sum_{n=0}^{\infty} \left( A_{0n}^{(2)} \right)^* x_n^h \right). \quad (\text{B41})$$

Imposing the normalization condition  $\tilde{P}_g + \tilde{P}_h = 1$ , the dynamics reduces to  $\dot{\tilde{P}}_g = -\gamma \tilde{P}_g + \tilde{P}_g^{\text{ss}}$ , where

$$\gamma \equiv \gamma_g + \gamma_h, \quad \tilde{P}_g^{\text{ss}} = \frac{\gamma_h}{\gamma}, \quad \tilde{P}_h^{\text{ss}} = \frac{\gamma_g}{\gamma}. \quad (\text{B42})$$

The rate equations remain unchanged when transformed back to the original frame, and describe the relaxation of the qubit populations toward a unique steady-state distribution  $\tilde{P}_g^{\text{ss}}$  and  $\tilde{P}_h^{\text{ss}}$ .

### B.III. Multi-Photon Resonances: Generalized Dynamics and Rate Equations

The perturbative approach in Sec. B.II can be generalized to multi-photon transitions. We consider a  $k$ -photon resonance between a lower state  $|g\rangle$  and some excited qubit state  $|j\rangle$ , with  $\omega_j - \omega_g \approx k\omega_r$ . The dominant dynamics may be captured by the effective Hamiltonian (up to higher-order corrections to the resonator energy),

$$\hat{H}_{\text{eff}} = \hat{H}^{(0)} + \hat{H}^{(1)}, \quad (\text{B43})$$

$$\hat{H}^{(0)} = \hat{\chi} \hat{a}^\dagger \hat{a} + \frac{1}{2} \delta_q \hat{\sigma}_z + \varepsilon_d \hat{a}^\dagger + \varepsilon_d^* \hat{a} + \text{const}, \quad (\text{B44})$$

$$\hat{H}^{(1)} = g_{\text{eff}}^{(k)} (\hat{a}^\dagger)^k \hat{\sigma}_- + (g_{\text{eff}}^{(k)})^* \hat{a}^k \hat{\sigma}_+. \quad (\text{B45})$$

The steady state of  $\hat{H}^{(0)}$  is the same as in Sec. B.I. Applying the same adiabatic elimination procedure as in Sec. B.II, we obtain the  $k$ -photon transition rates

$$\gamma_g^{(k)} = -2|g_{\text{eff}}^{(k)}|^2 \operatorname{Re} \left( \sum_{n=0}^{\infty} (A_{n0}^{(k)})^* x_n^g \right), \quad (\text{B46})$$

$$\gamma_j^{(k)} = -2|g_{\text{eff}}^{(k)}|^2 \operatorname{Re} \left( \sum_{n=0}^{\infty} (A_{0n}^{(k)})^* x_n^j \right), \quad (\text{B47})$$

where

$$x_n^g = \sum_{m=n}^{\infty} (-1)^{m-n} \frac{A_{m0}^{(k)}}{c_{m0}^{00}} \left( \prod_{\ell=n}^{m-1} \frac{c_{\ell0}^{10}}{c_{\ell0}^{00}} \right), \quad (\text{B48})$$

$$x_n^j = \sum_{m=n}^{\infty} (-1)^{m-n} \frac{A_{0m}^{(k)}}{c_{0m}^{00}} \left( \prod_{\ell=n}^{m-1} \frac{c_{0\ell}^{01}}{c_{0\ell}^{00}} \right). \quad (\text{B49})$$

The coefficients  $A_{nm}^{(k)}$  and  $c_{nm}^{ab}$  follow expressions similar to those in Sec. B.II with  $k$ -photon generalization, allowing one to describe the relaxation dynamics between  $|g\rangle$  and  $|j\rangle$ .

### C. NUMERICAL SIMULATIONS SETUP

In this section, we describe the simulation setup and analysis methods used for the numerical results in the main text. All quantum simulations are implemented in QuTiP [5]. In the main text, we simulate the system with photon truncation number  $n^{\max} = 100$ , and qubit truncation number  $j^{\max} = 4$ . For the reduced model, we use a qubit subspace spanned by  $\{|g\rangle = |0\rangle, |h\rangle = |3\rangle\}$ , corresponding to the two-photon resonance  $\omega_h - \omega_g \approx 2\omega_r$ .

#### C.I. Model Comparisons

We compare dynamics from the full quantum model [6] and from a semiclassical approximation including measurement backaction [7]. In our simulations, this version of the semiclassical model shows closer agreement with the full quantum results than the backaction-free version.

For the full quantum model, the evolution follows the master equation, Eq. (A6). In the semiclassical model, the resonator operators are replaced by their expectation values,  $\alpha(t) = \langle \hat{a} \rangle = \operatorname{Tr}(\hat{a} \hat{\rho})$ , leading to the equation of motion

$$\dot{\alpha} = -i\omega_r \alpha + g\langle \hat{n} \rangle - 2 \sin(\omega_d) \varepsilon_d \hat{a} - \frac{\kappa}{2} \alpha. \quad (\text{C1})$$

Substituting  $\hat{a} \rightarrow \alpha$  and  $\hat{a}^\dagger \rightarrow \alpha^*$  in  $\hat{H}_{\text{full}}$  yields a time-dependent qubit Hamiltonian,

$$\hat{H}_{\text{sc}}(t) = \hat{H}_q + 2g\hat{n} \operatorname{Im}\{\alpha(t)\}, \quad (\text{C2})$$

$$i\frac{\partial}{\partial t} |\psi_{\text{sc}}(t)\rangle = \hat{H}_{\text{sc}}(t) |\psi_{\text{sc}}(t)\rangle. \quad (\text{C3})$$

#### C.II. Time Evolution Simulation Settings

For each model, we apply a different numerical method for the time evolution simulation. For the full model, whose large Hilbert space and fast dynamics make direct integration expensive, we use the QuTiP Monte Carlo solver to solve the full master equation [Eq. (A6)] (using 200 trajectories for  $\varepsilon_d \leq 12\text{MHz}$ , and 400 trajectories for  $\varepsilon_d > 12\text{MHz}$ .) For the reduced model, we use the QuTiP master equation solver to integrate the master equation of the reduced quantum model [Eq. (A34)]. For the semiclassical model, we use a custom ODE solver to evolve the coupled nonlinear equations [Eqs. (C1) and (C3)]. A summary of the solvers, time steps, and truncations is given in Table C1.

Different initial states are used for the quantum and semiclassical models, reflecting their distinct treatments of the resonator mode. To ensure consistency between the quantum models, we initialize the reduced quantum model in the

state  $|g, 0\rangle$  of its SW-transformed frame, while in the full model we use  $\widetilde{|g, 0\rangle} = e^{-\hat{S}}|g, 0\rangle$ , which corresponds to the same physical ground state expressed in the laboratory frame. For the semiclassical model, the initial qubit state is  $|g\rangle$  with the resonator coherent-state amplitude set to  $\alpha = 0$ .

Model	Full Quantum Model	Reduced Quantum Model	Semiclassical Model
Solver	QuTiP Monte-Carlo solver ( $\varepsilon_d \leq 12\text{MHz}$ : 200 trajectories $\varepsilon_d > 12\text{MHz}$ : 400 trajectories)	QuTiP master equation solver	Custom ODE solver
Time step (ns)	2.5	2.5	2.5
$n^{\max}$	100	100	—
$j^{\max}$	4	—	4

TABLE C1. Numerical simulation settings for different models.

### C.III. Numerical Extraction of Relaxation Rates

To extract the relaxation rates in Fig. 2(a) of the main text, we first obtain the steady-state solution of the master equation [Eq. (A34)] using the steady-state solver in QuTiP. This yields the steady-state dressed-state populations  $\tilde{P}_{g/h}^{\text{ss}}$ . We then perform a time-evolution simulation of the reduced model to obtain  $\tilde{P}_{g/h}(t)$  and fit the results to the exponential form

$$\tilde{P}_{g/h}(t) = \tilde{P}_{g/h}^{\text{ss}} + C_{g/h} e^{-\gamma t}, \quad (\text{C4})$$

where  $C_{g/h}$  is a time-independent constant determined by the initial conditions. To avoid transient bias, only data with  $t > t_{\min} \approx 10/\kappa$  are included. For improved accuracy, we initialize the system in  $|h, 0\rangle$  when  $\varepsilon_d/2\pi \leq 7\text{MHz}$  and in  $|g, 0\rangle$  otherwise, so that the fitted coefficient  $C_{g/h}$  is sufficiently large for accurate extraction.

### C.IV. Estimation of Dressed-State Populations

Given the analytically obtained relaxation rate  $\gamma$  and steady-state populations  $\tilde{P}_{g/h}^{\text{ss}}$  from Sec. B.II, the dressed-state populations at any time  $t$  can be estimated using Eq. (C4). For the initial state  $|g, 0\rangle$ , which gives  $\tilde{P}_g(0) = 1$ ,

$$\tilde{P}_{g/h}(t) \approx \tilde{P}_{g/h}^{\text{ss}} + [1 - \tilde{P}_{g/h}^{\text{ss}}] e^{-\gamma t}. \quad (\text{C5})$$

This expression is used to generate the curves shown in Fig. 4(d) of the main text.

---

\* chiaowang@phys.ntu.edu.tw

- [1] J. R. Schrieffer and P. A. Wolff, [Phys. Rev. \*\*149\*\*, 491 \(1966\)](#).
- [2] A. Blais, J. Gambetta, A. Wallraff, D. I. Schuster, S. M. Girvin, M. H. Devoret, and R. J. Schoelkopf, [Phys. Rev. A \*\*75\*\*, 032329 \(2007\)](#).
- [3] A. Blais, A. L. Grimsmo, S. M. Girvin, and A. Wallraff, [Rev. Mod. Phys. \*\*93\*\*, 025005 \(2021\)](#).
- [4] W. Magnus, [Commun. Pure Appl. Math. \*\*7\*\*, 649 \(1954\)](#).
- [5] N. Lambert, E. Giguère, P. Menczel, B. Li, P. Hopf, G. Suárez, M. Gali, J. Lishman, R. Gadhvi, R. Agarwal, A. Galicia, N. Shammah, P. Nation, J. R. Johansson, S. Ahmed, S. Cross, A. Pitchford, and F. Nori, [arXiv:2412.04705](#).
- [6] M. F. Dumas, B. Groleau-Paré, A. McDonald, M. H. Muñoz-Arias, C. Lledó, B. D’Anjou, and A. Blais, [Phys. Rev. X \*\*14\*\*, 041023 \(2024\)](#).
- [7] Z. Wang, B. D’Anjou, P. Gigon, A. Blais, and M. S. Blok, [arXiv:2505.00639](#).